Supporting Information

Multi-Element Metal Oxide Ultra-small-sized Nanofibers: An Efficient Electrocatalyst for Hydrogen Evolution

Peng Liu[a], *Changchun Sun*[a], *Guiju Liu*[b], *Zhan Jiang*[a,*], *Haiguang Zhao*[a,b,*]

[a] College of Textiles & Clothing, Qingdao University, No. 308 Ningxia Road, Qingdao 266071, P.R. China

[b] College of Physics and State Key Laboratory of Bio-Fibers and Eco-Textiles, Qingdao University, No. 308 Ningxia Road, Qingdao 266071, P.R. China

[*]Corresponding author. Email: kevinjiang_1987@126.com; hgzhao@qdu.edu.cn

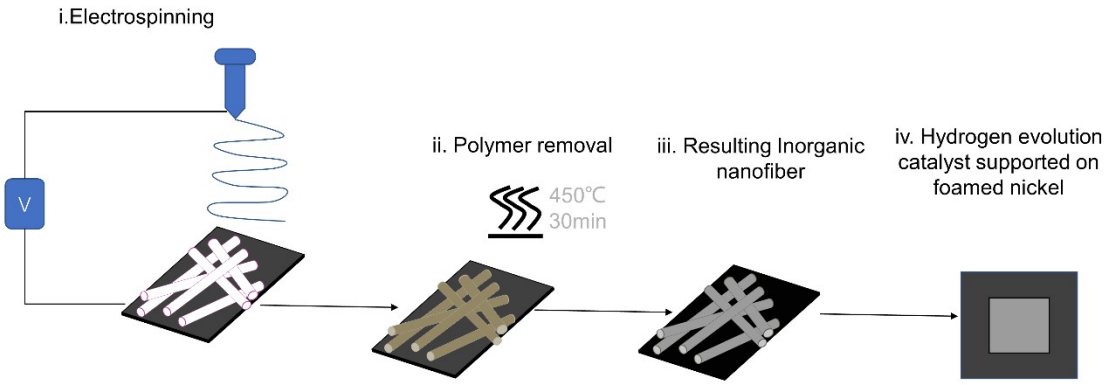

Figure S1. Scheme showing the methodology we used in this work for fabricating the metal oxide nanofibers.

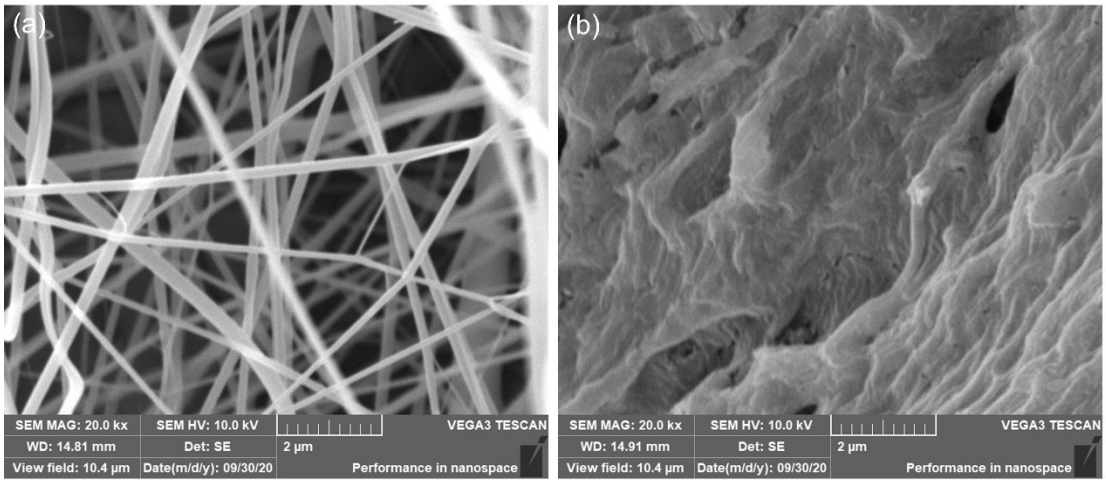

Figure S2 SEM images of CoO sample: (a) before and (b) after sintering at 450 ℃.

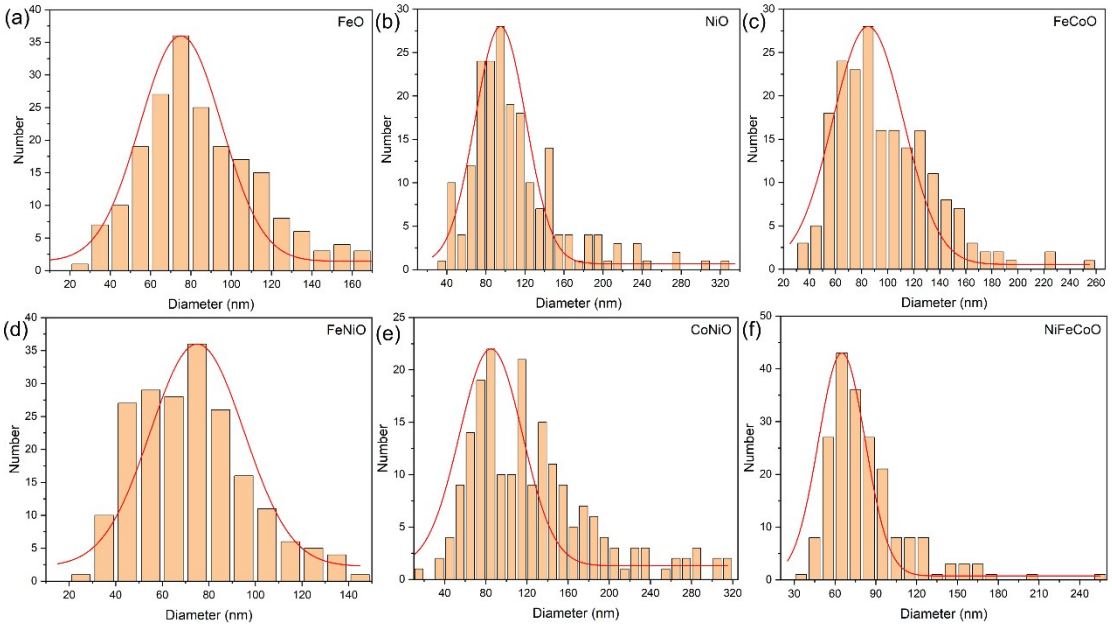

Figure S3. Diameters of the FeO, NiO, FeCoO, FeNiO, CoNiO, and NiFeCoO nanofibers.

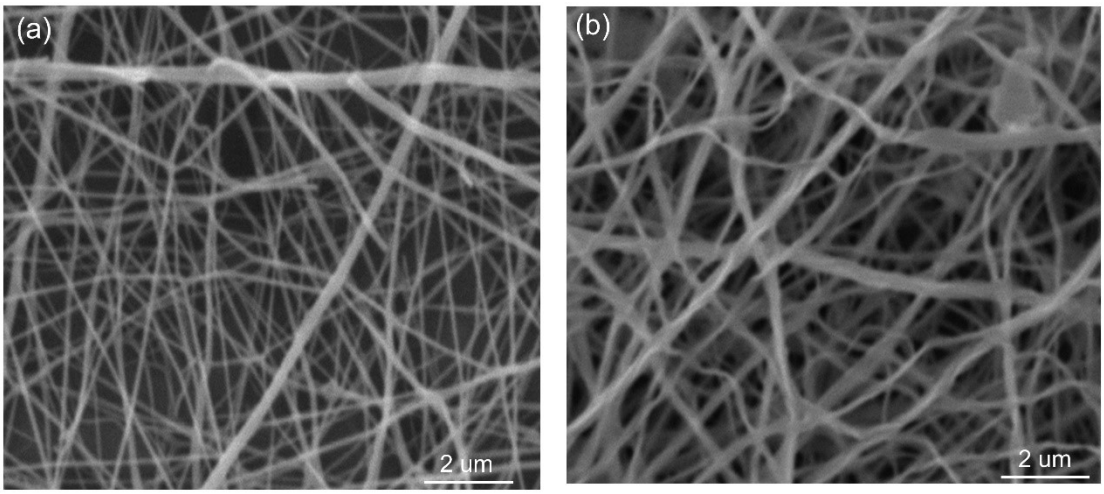

Figure S4. SEM images of (a) FeO and (b) NiO samples.

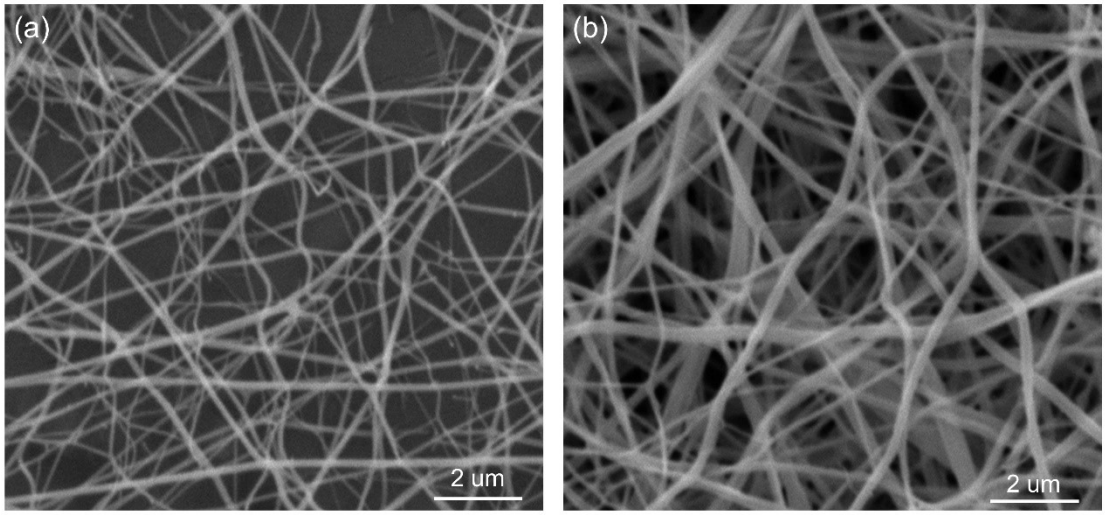

Figure S5. SEM images of (a) FeNiO and (b) CoNiO samples.

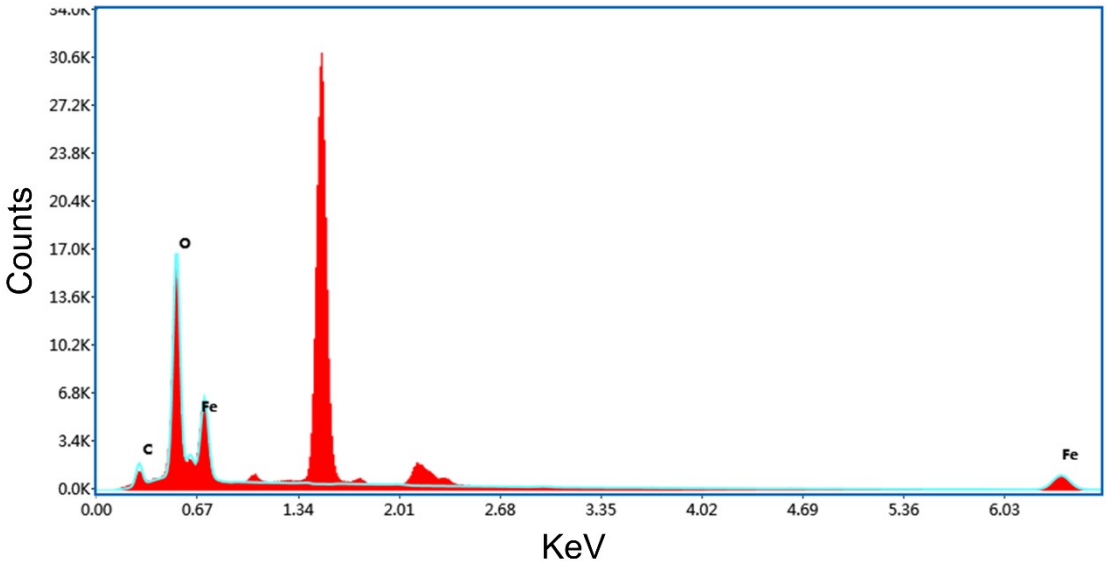

Figure S6.EDX spectrum of the FeO sample.

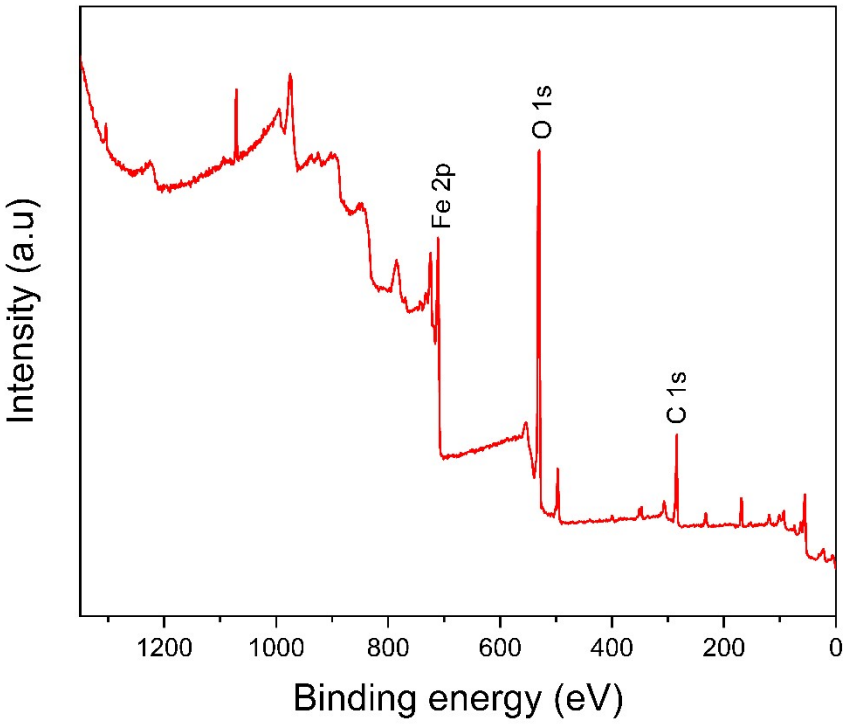

Figure S7. Typical XPS survey spectrum of FeO sample.

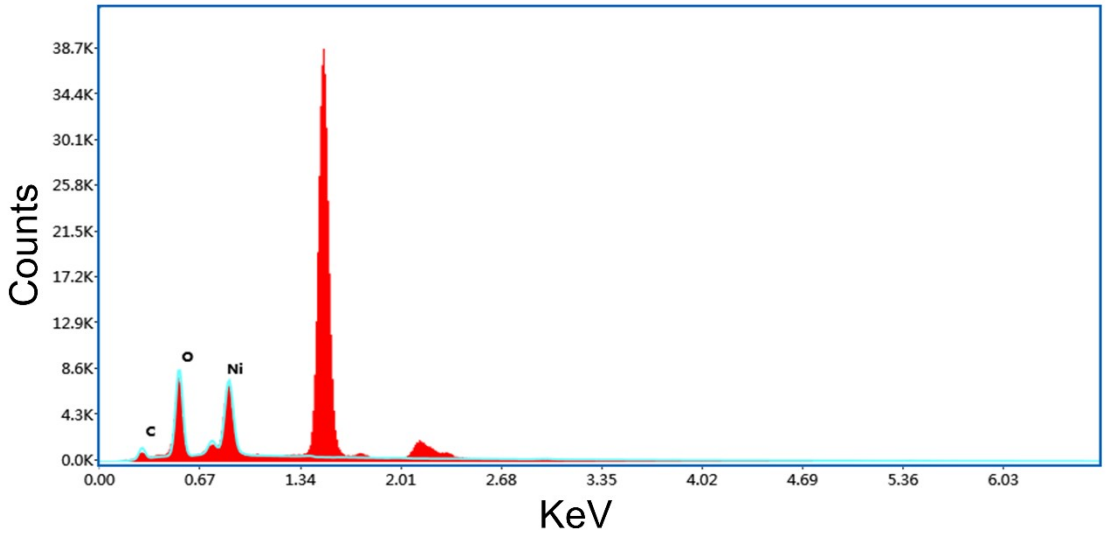

Figure S8.EDX spectrum of the NiO sample.

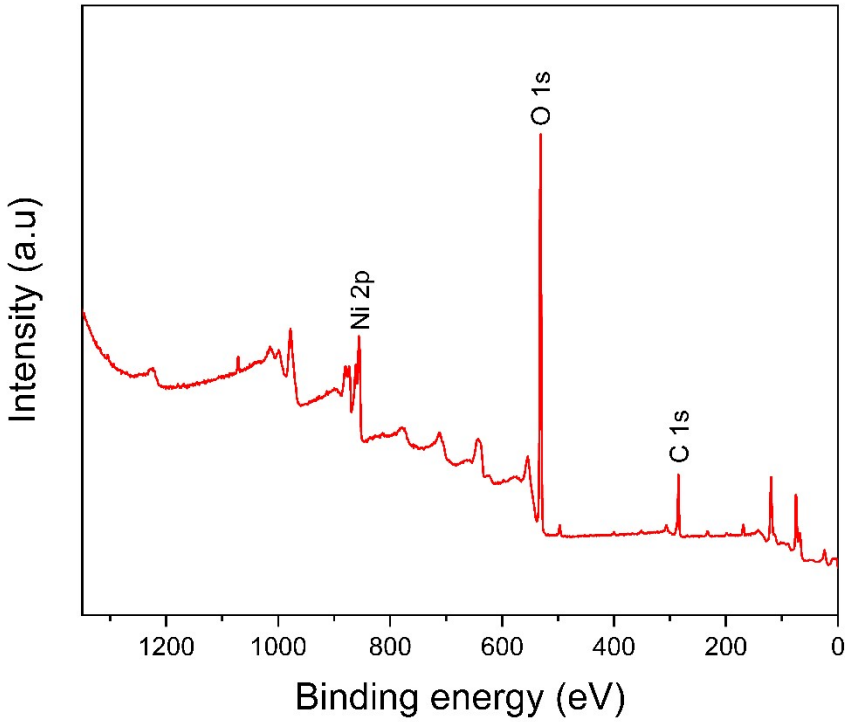

Figure S9. Typical XPS survey spectrum of NiO sample.

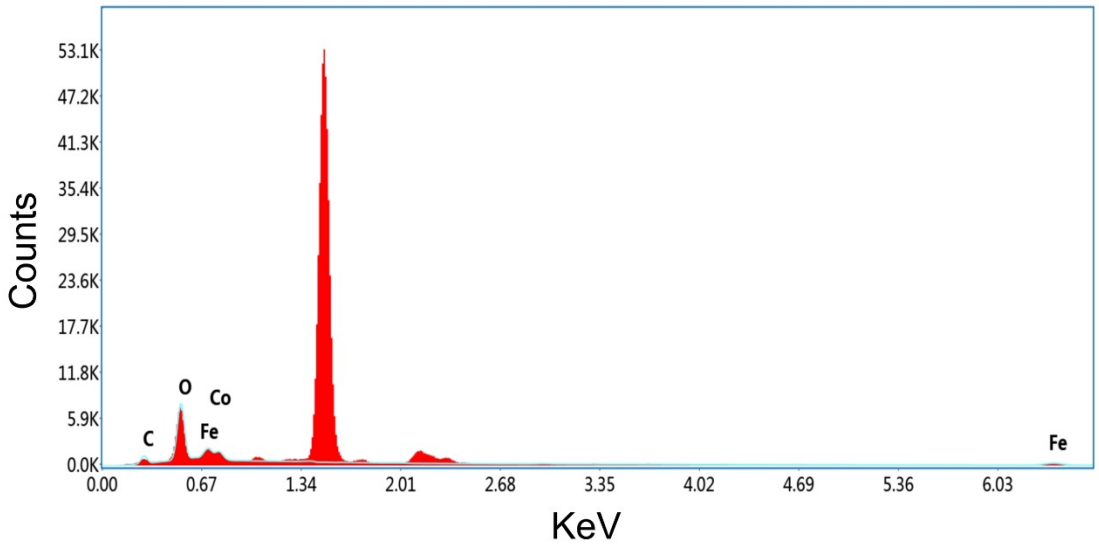

Figure S10.EDX spectrum of the FeCoO sample.

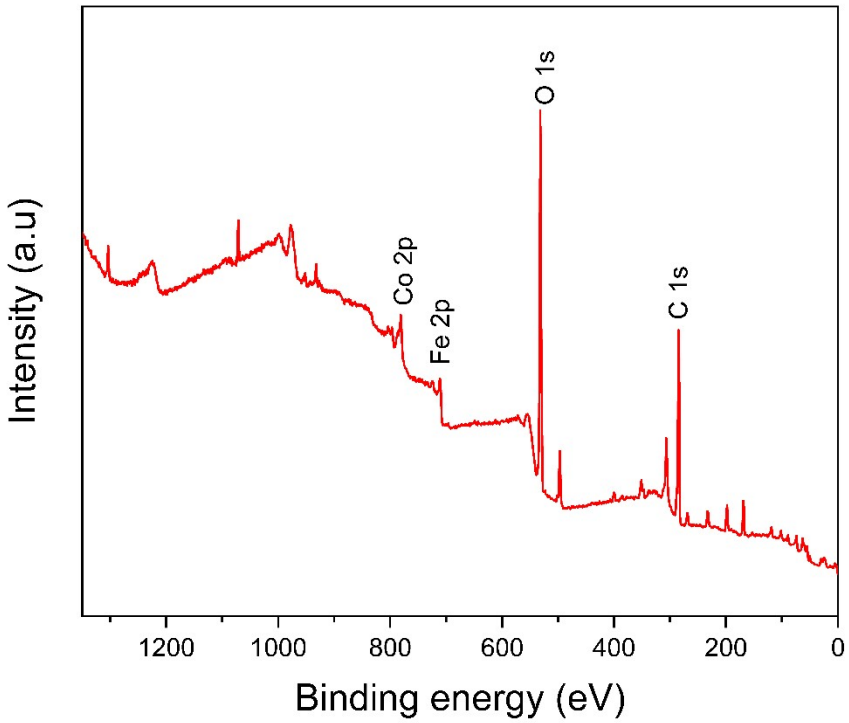

Figure S11. Typical XPS survey spectrum of FeCoO sample.

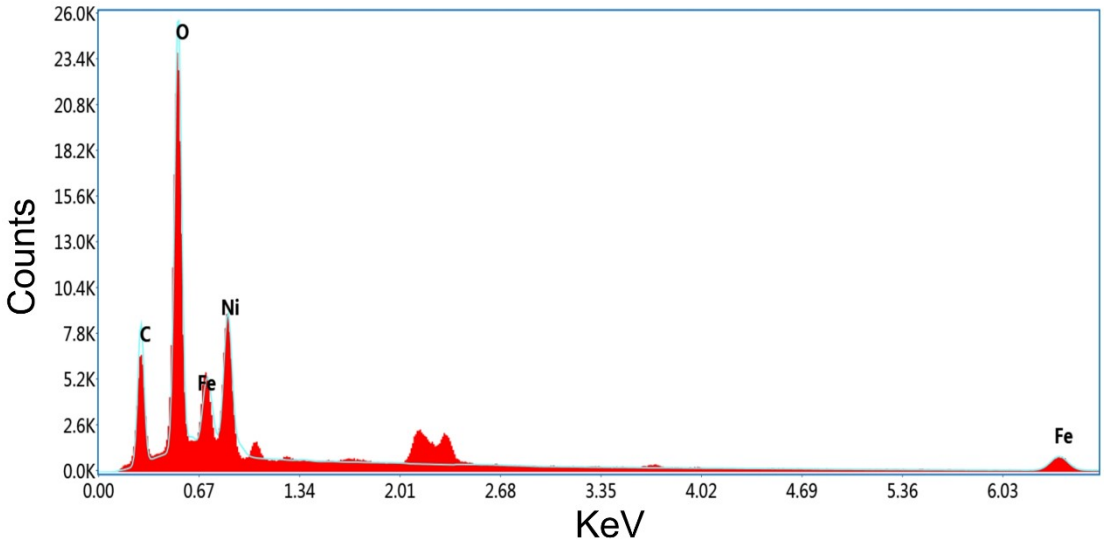

Figure S12.EDX spectrum of the FeNiO sample.

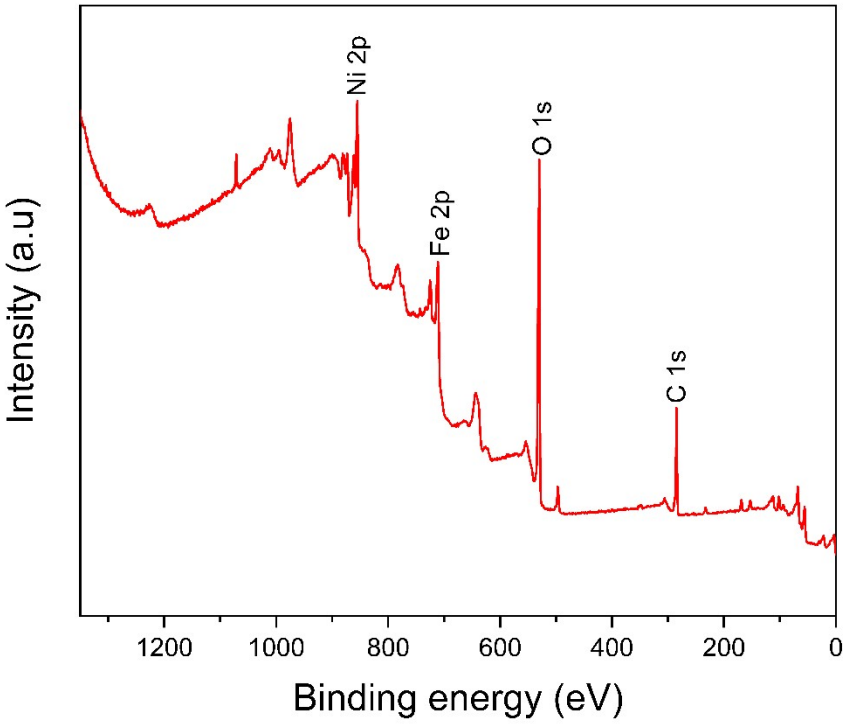

Figure S13. Typical XPS survey spectrum of FeNiO sample.

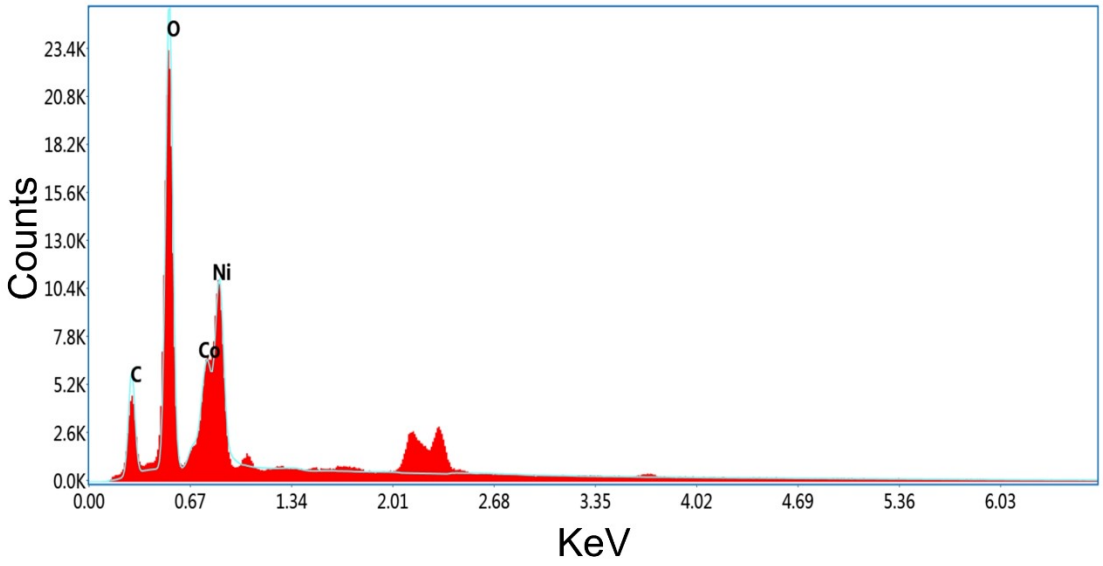

Figure S14.EDX spectrum of the CoNiO sample.

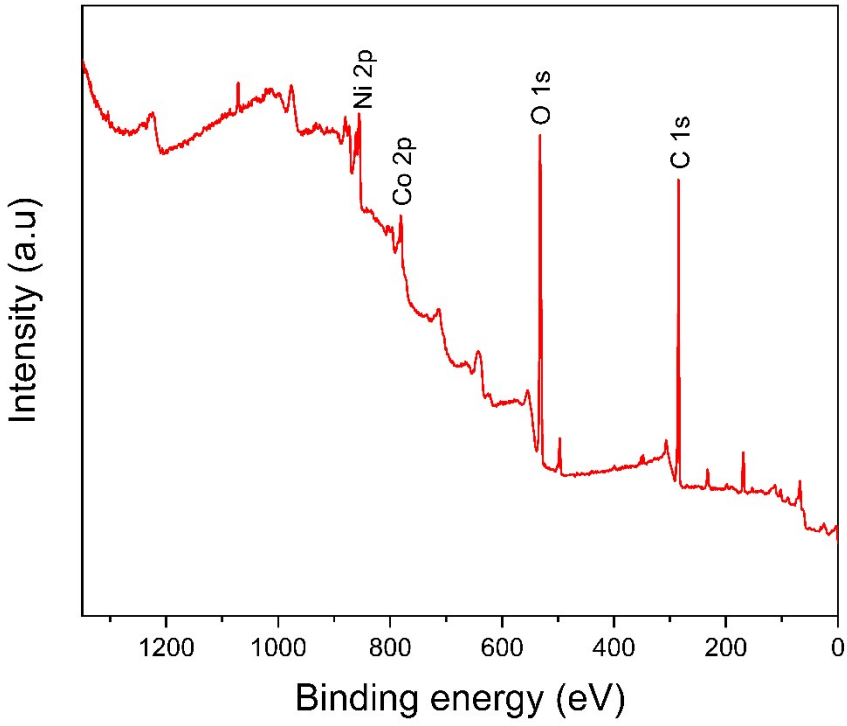

Figure S15. Typical XPS survey spectrum of CoNiO sample.

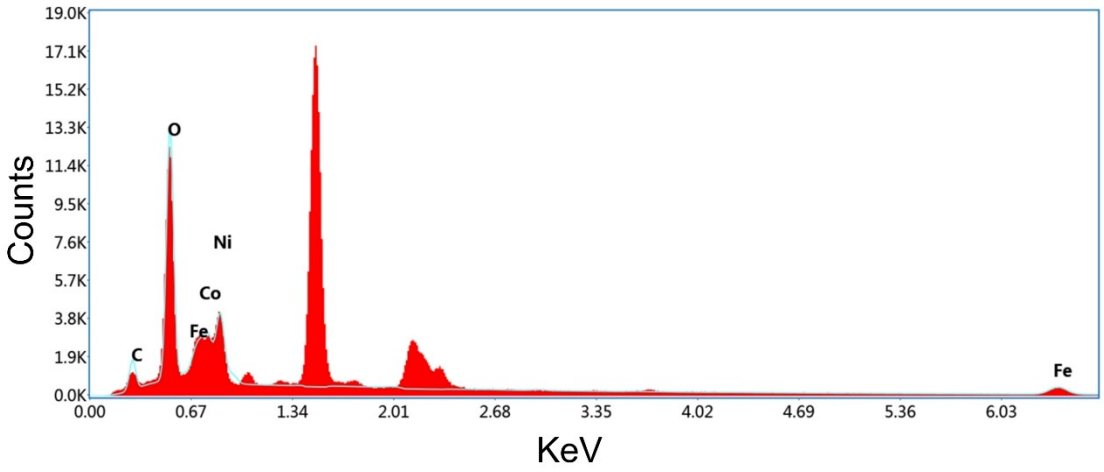

Figure S16.EDX spectrum of the NiFeCoO sample.

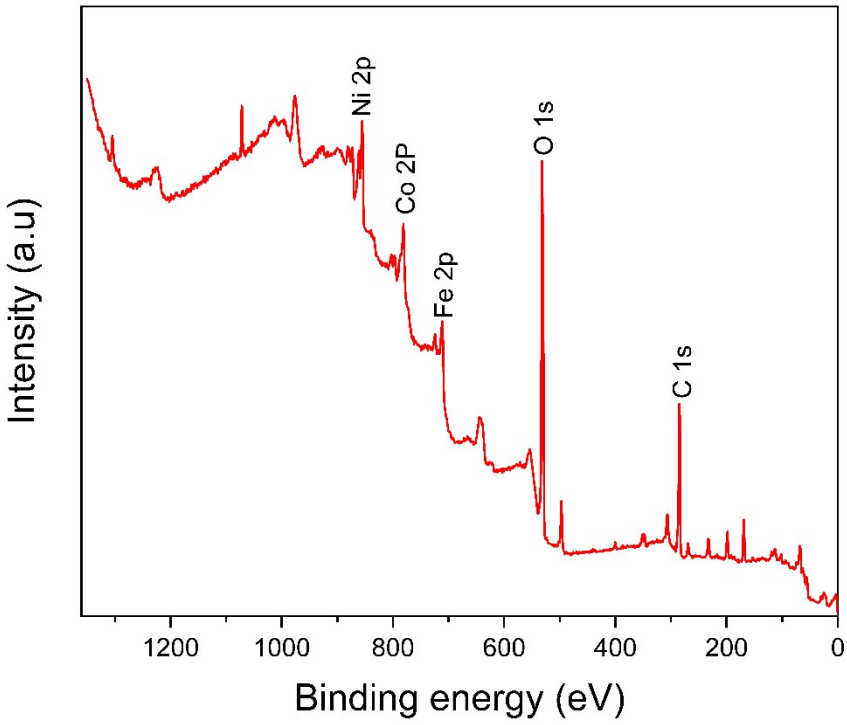

Figure S17. Typical XPS survey spectrum of NiFeCoO sample.

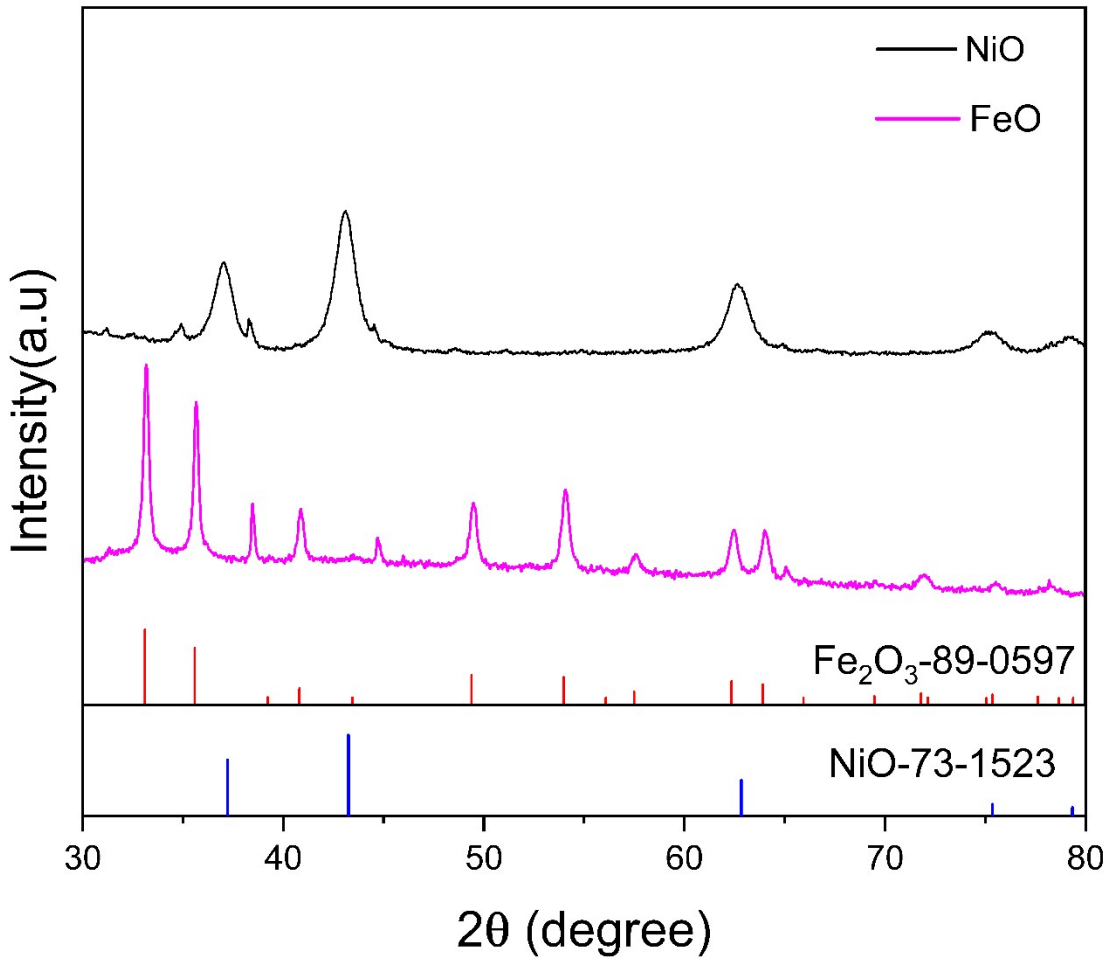

Figure S18. XRD patterns of FeO and NiO samples.

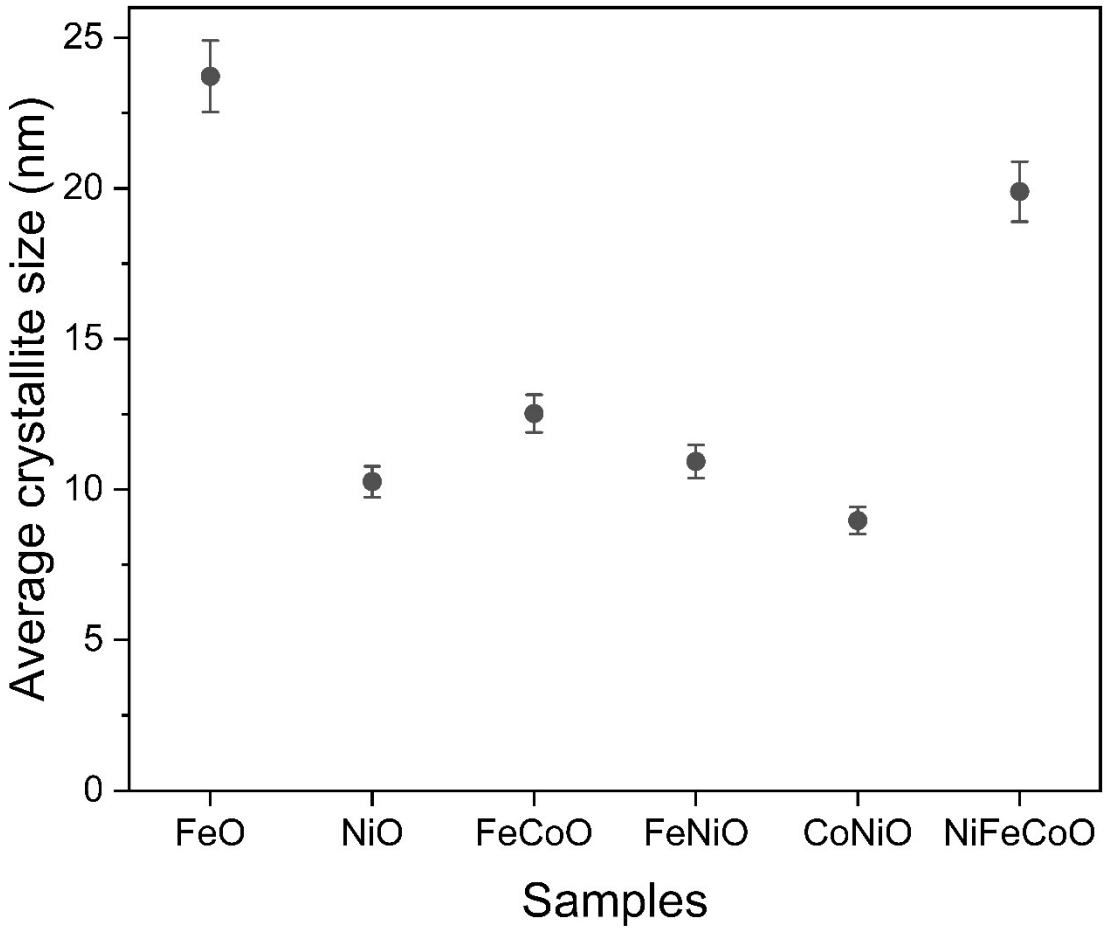

Figure S19. Average crystallite size of the FeO, NiO, FeCoO, FeNiO, CoNiO, and NiFeCoO samples.

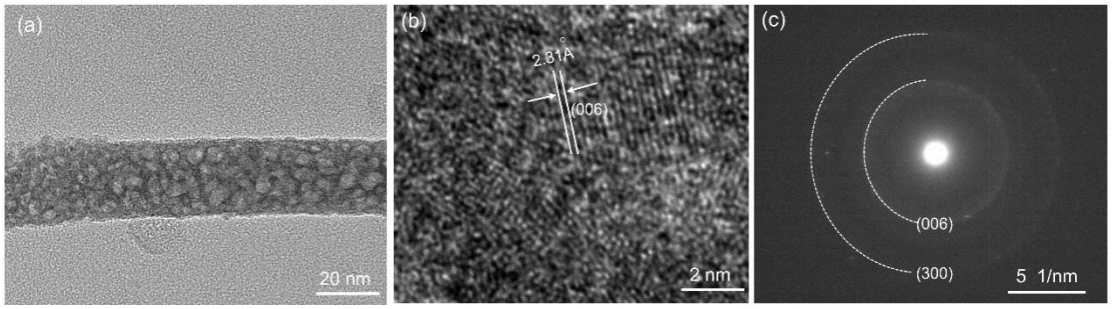

Figure S20. (a) TEM image of FeO sample. (b) HRTEM image of FeO sample. (c) SAED of FeO sample.

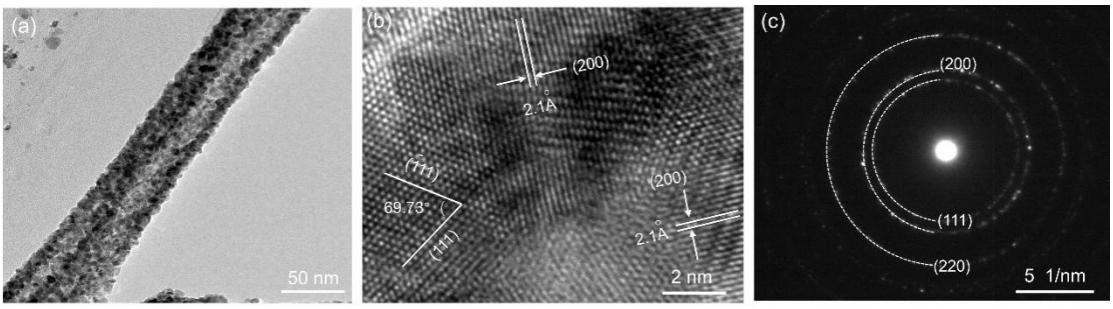

Figure S21. (a) TEM image of NiO sample. (b) HRTEM image of NiO sample. (c) SAED of NiO sample.

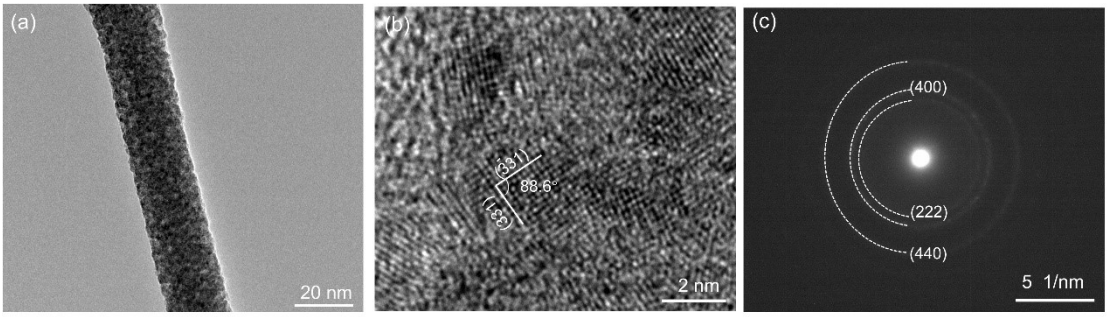

Figure S22. (a) TEM image of FeNiO sample. (b) HRTEM image of FeNiO sample. (c) SAED of FeNiO sample.

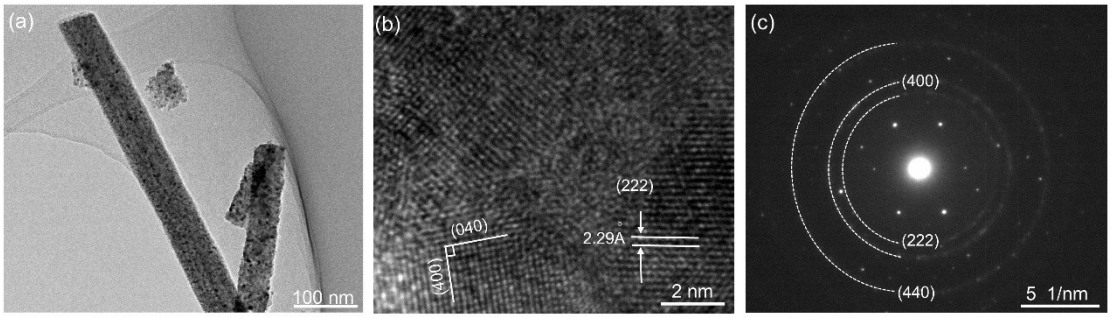

Figure S23. (a) TEM image of CoNiO sample. (b) HRTEM image of CoNiO sample. (c) SAED of CoNiO sample.

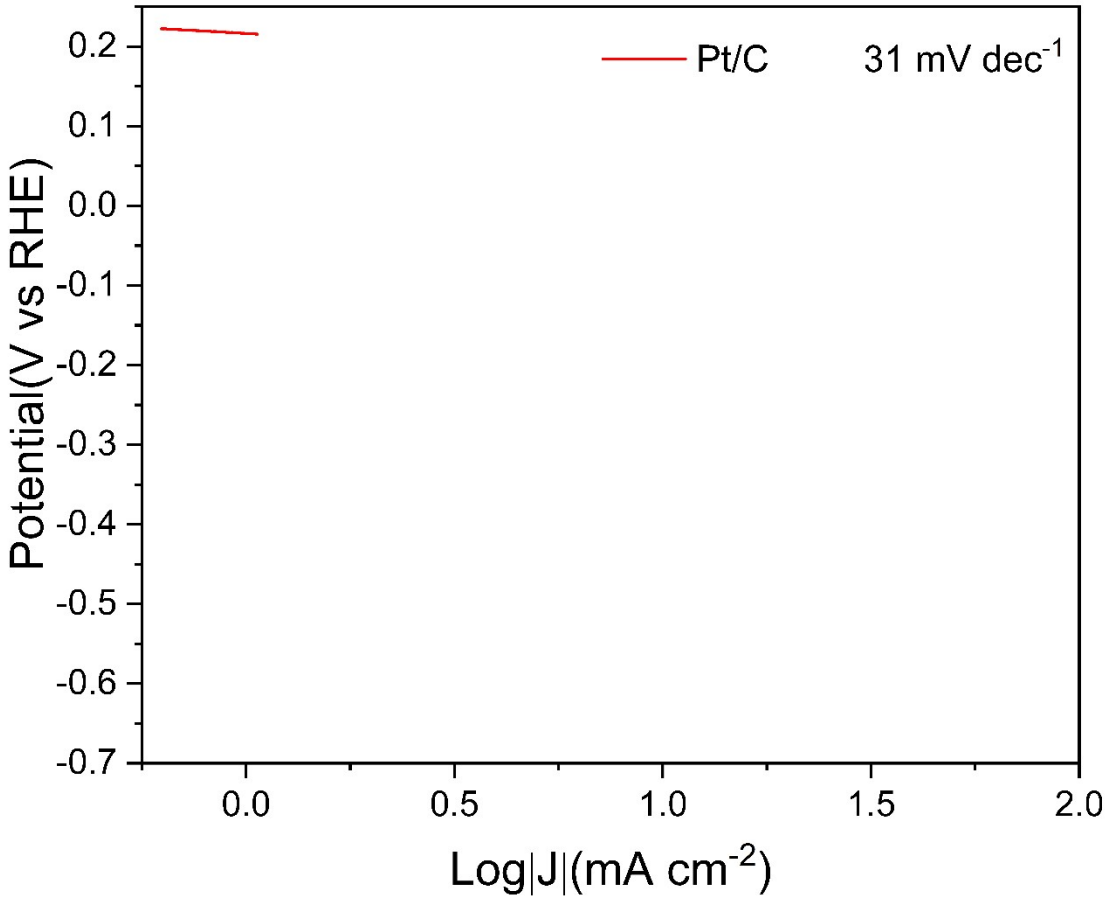

Figure S24. Tafel plots of Pt/C in 1.0 M KOH.

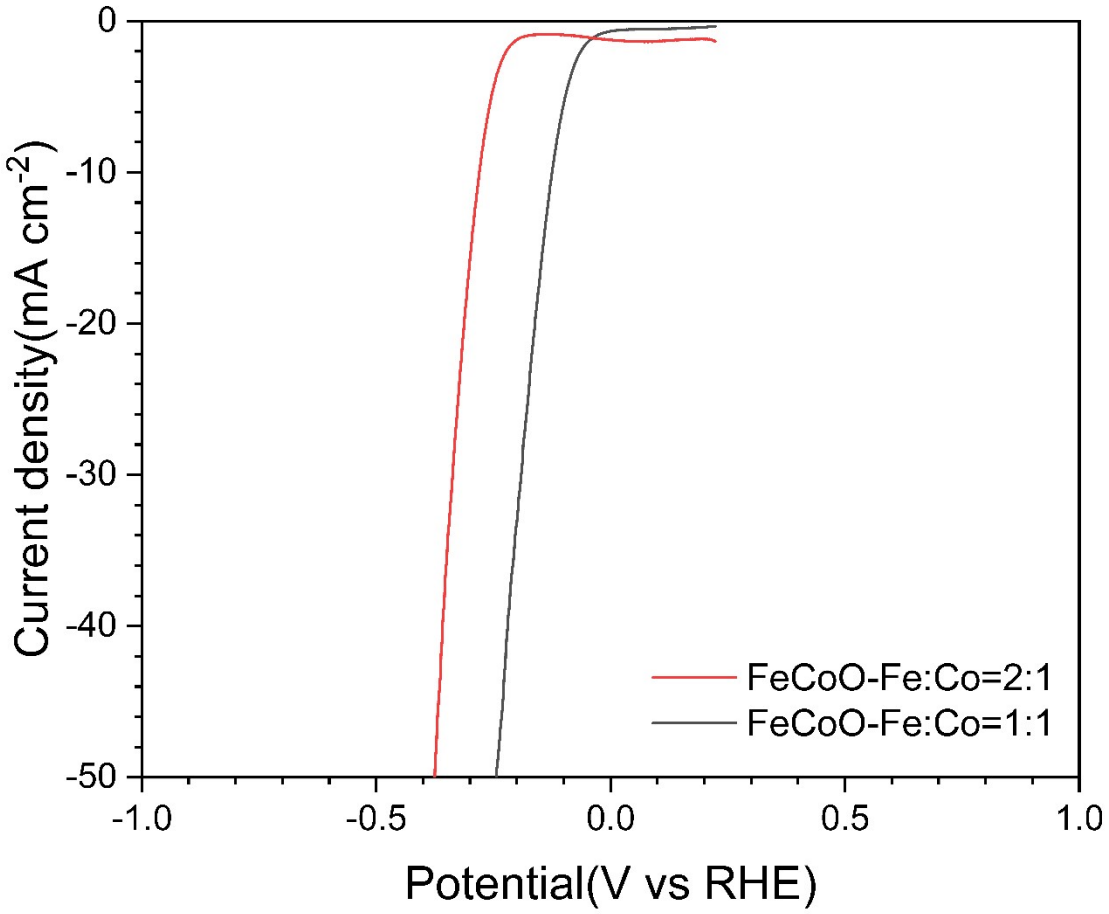

Figure S25. Polarization curves for FeCoO samples with identical Fe content, but different cobalt contents in 1.0 M KOH.

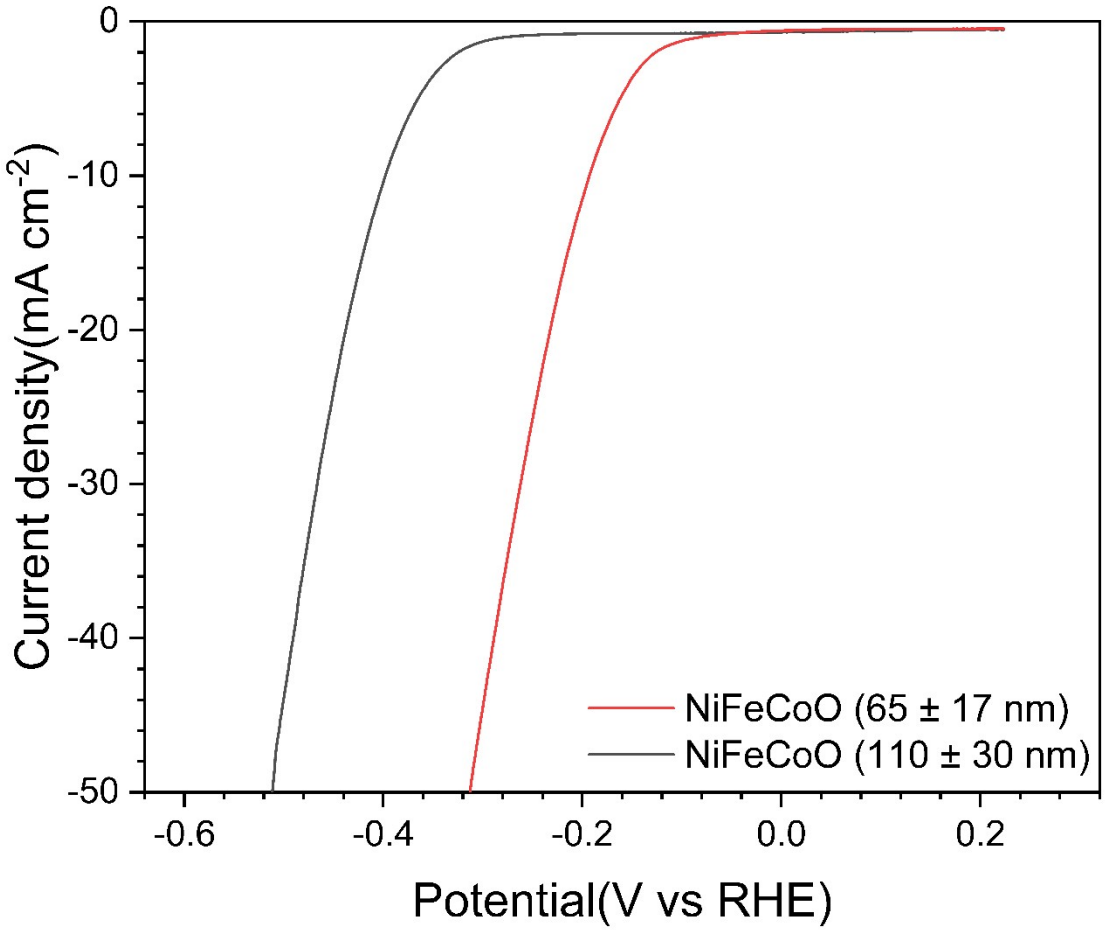

Figure S26. Polarization curves for NiFeCoO samples with different fiber diameters in 1.0 M KOH.

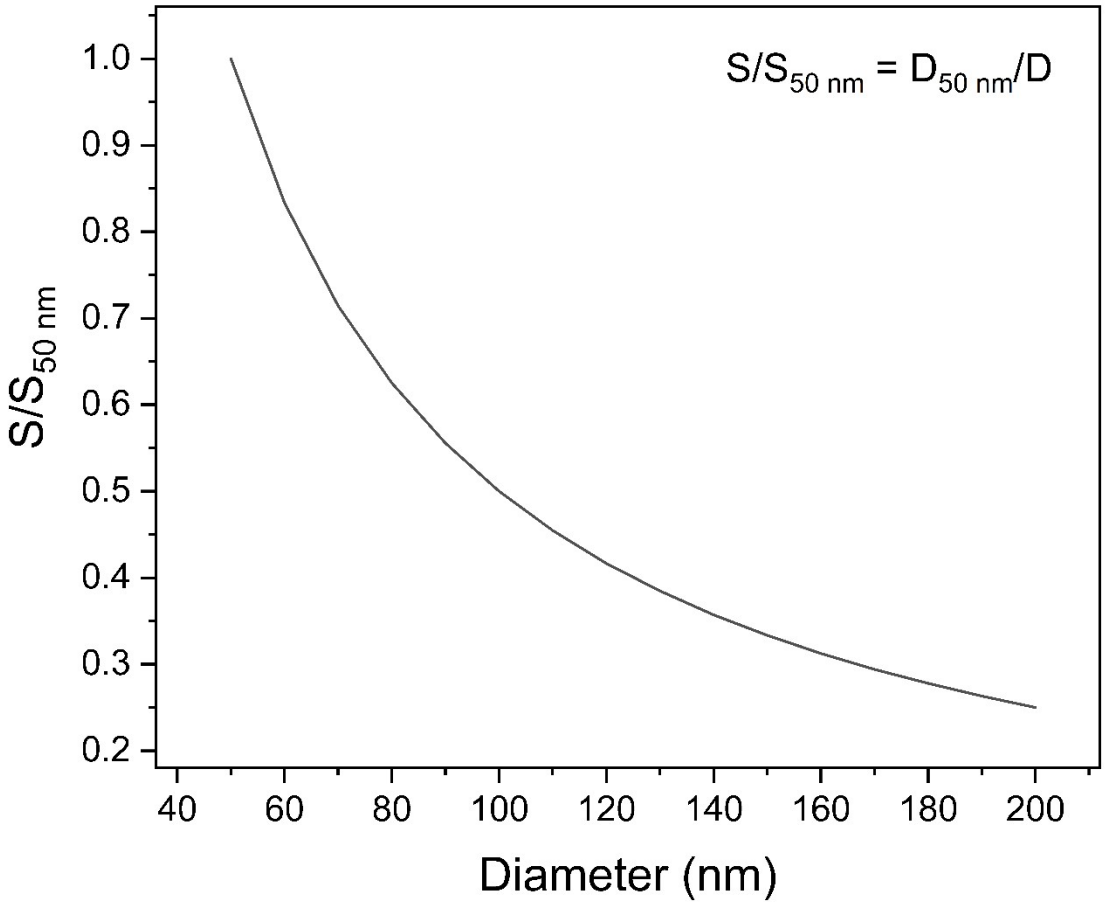

Figure S27. The relationship between specific surface area (compared to the surface area of fibers with diameter of 50 nm, $S_{50\ nm}$) and fiber diameter.

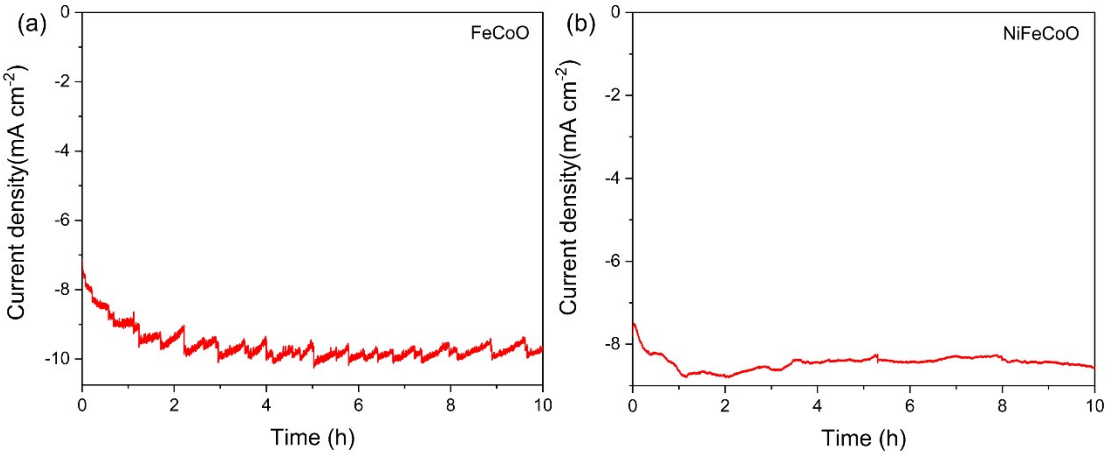

Figure S28. Chronopotentiometric curves for (a) FeCoO and (b) NiFeCoO sample in 1.0 M KOH.

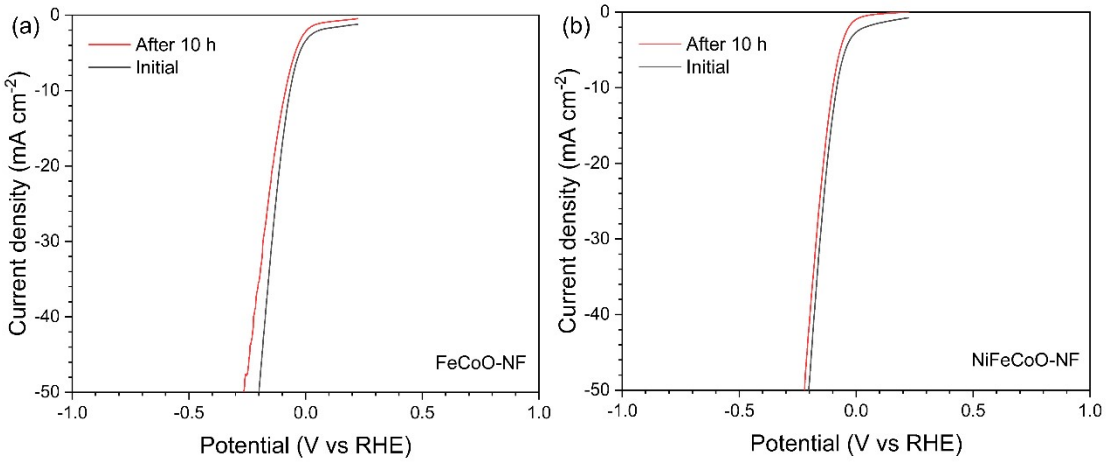

Figure S29. Polarization curves for (a) FeCoO-NF and (b) NiFeCoO-NF sample in 1.0 M KOH after 10 h operation.

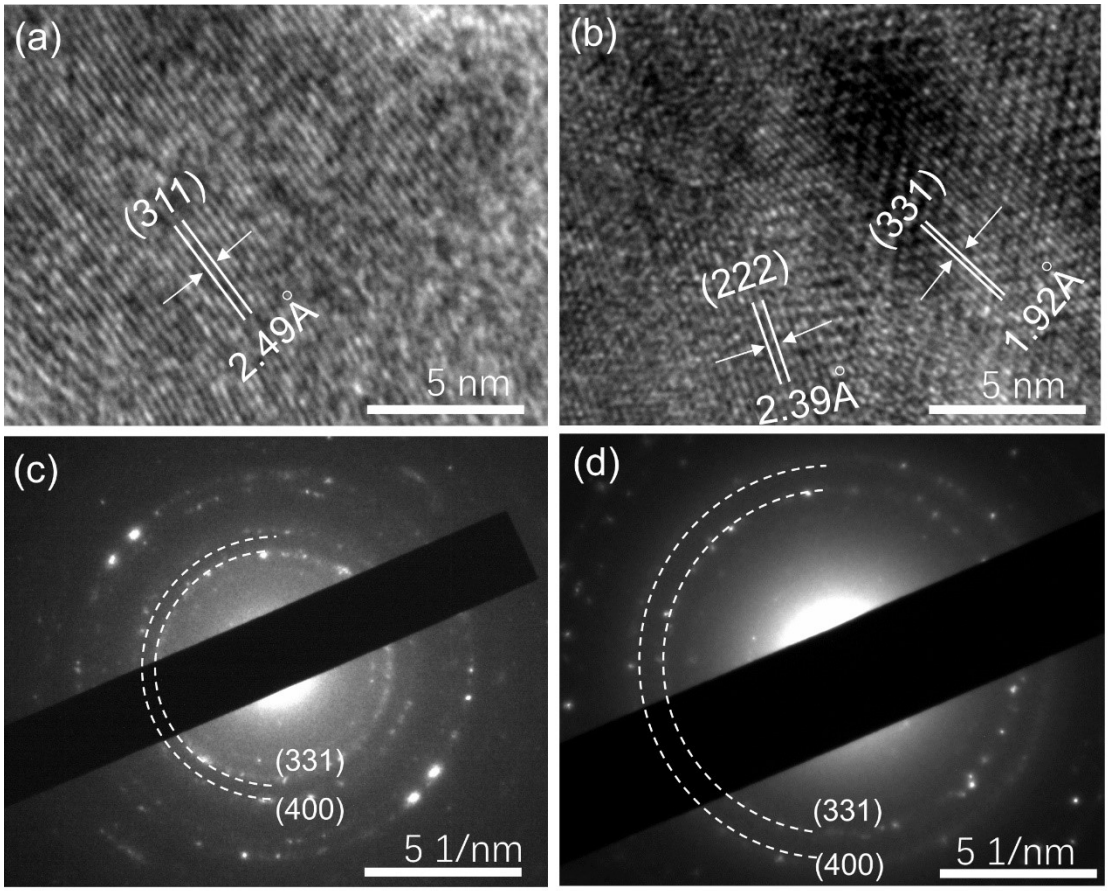

Figure S30. HRTEM images of (a) FeCoO and (b) NiFeCoO samples. SAED of (c) FeCoO and (d) NiFeCoO samples after 10 hours of electrochemical testing.

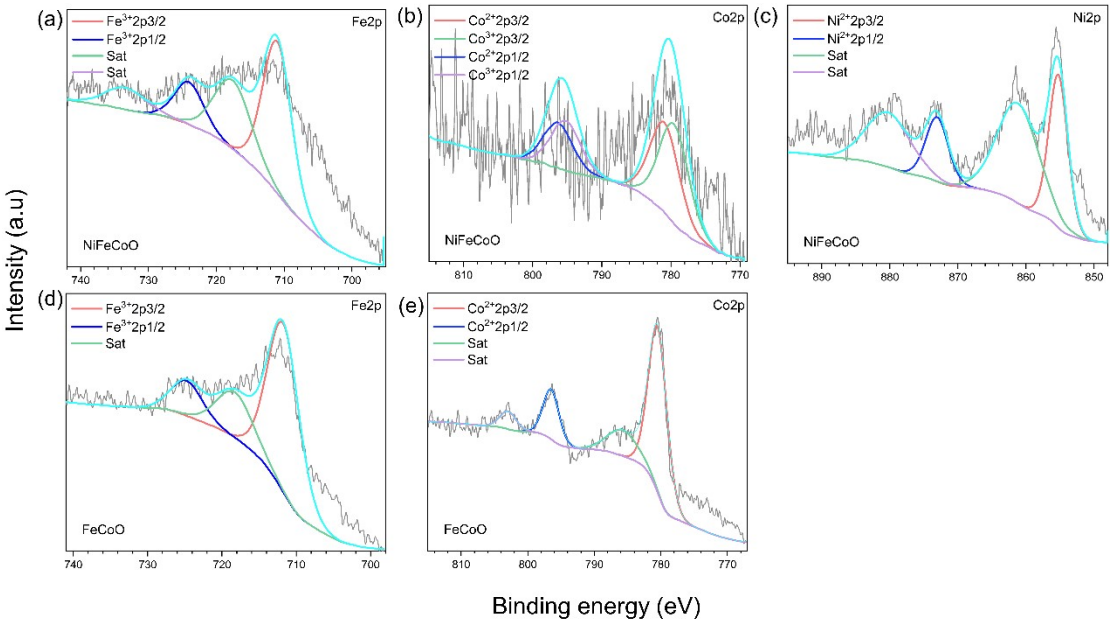

Figure S31. After 10 hours of electrochemical testing: (a-c) Fe 2p, Co 2p and Ni 2p high-resolution XPS spectra of the NiFeCoO sample. (d-e) Fe 2p and Co 2p high-resolution XPS spectra of the FeCoO sample.

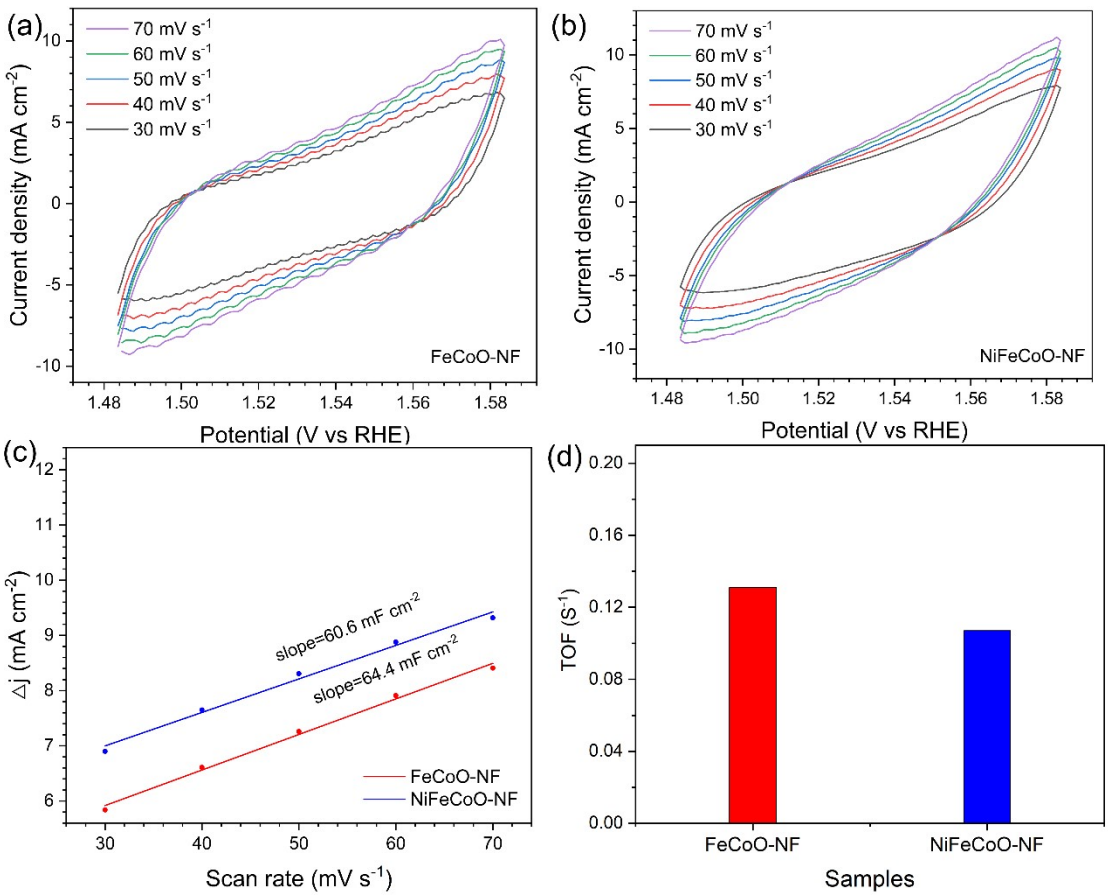

Figure S32. (a-b) CV curves of FeCoO-NF and NiFeCoO-NF samples at various scan rates (30, 40, 50, 60, and 70 mV s^{-1}) in the potential range of 1.48~1.58 V (vs RHE). (c) Scan rate dependence of the current densities of FeCoO-NF and NiFeCoO-NF at 1.53 V vs. RHE. (d) TOF (at an overpotential of 100 mV) for FeCoO-NF and NiFeCoO-NF samples.

Assuming a one-electron process for both reduction and oxidation, the upper limit of active sites for FeCoO-NF and NiFeCoO-NF can be calculated from CV according to the follow Equation (S1)：

$$n = \frac{Q}{2F} \tag{S1}$$

where n is the number of active sites, F is the Faraday constant, and Q is the whole charge of CV curve at 50 mV s^{-1}, respectively.

Assuming that all of active sites were entirely accessible to the electrolyte, the following formula was used to calculate TOF (Equation (S2)):

$$TOF = \frac{I}{2nF} \tag{S2}$$

where F and n are the Faraday constant and the number of active sites, respectively; I is the current of LSV curves.

Table S1. Summary of the HER catalytic activity of representative catalysts.

Catalysts	η_{10} [mA cm^{-2}]	Tafel slope [mA cm^{-2}]	Ref
Co_3O_4 nanoarray	73	85	[1]
NiOx@BCNTs	79	119	[2]
Co/ Co_3O_4	90	44	[3]
Ni/NiFe-LDO	29	82	[4]
NiO/Ni heterostructures	88	115	[5]
P-Fe_3O_4/IF	42	41.9	[6]
FeCoO-NF	205	118	[7]
CoFeNi-O	57.6	40.7	[8]
CoOx@CN	232	115	[9]
Ni-Fe NPs (Ni_5Fe_1)	46	58	[10]
P-NCO NWs/NF	55	144.92	[11]
NiFe/$NiCo_2O_4$/NF	105	88	[12]
S-CoO NRs	73	82	[13]
NG5-Ar	190	45	[14]
NiO/Ni-CNT	80	82	[15]
CoO/Fe_3O_4	220	73	[16]
Ni_2P/ $NiCo_2O_4$	45	45	[17]
$NiFe_2O_4$	300	125	[18]
NP-$NiCo_2O_4$	370	123	[19]
Ni/Co_3O_4	145	109	[20]
Ni/NiO/Fe_3O_4	206	57	[21]
$NiCo_2O_4$NSs	180	63	[22]
Co/CoO	158	68	[23]
NiFeCoO-NF	42	56	This work
FeCoO-NF	66	130	This work

Table S2. The average diameter of the FeO, NiO, FeCoO, FeNiO, CoNiO, and NiFeCoO nanofibers.

Sample	Average diameter (nm)
NiFeCoO	65 ± 17
FeCoO	85 ± 27
FeNiO	75 ± 20
CoNiO	85 ± 30
FeO	75 ± 20
NiO	95 ± 26

Table S3. Element molar ratio of binary and ternary sample in EDX spectrum and XPS survey spectrum.

Sample	EDX spectrum element molar ratio	XPS survey spectrum element molar ratio
NiFeCoO	Fe:Co:Ni =1:1.22:2.36	Fe:Co:Ni=1.16:1.31:1
FeCoO	Fe:Co =1.05:1	Fe:Co =1:1.39
FeNiO	Fe:Ni =1:2.24	Fe:Ni =1.66:1
CoNiO	Co:Ni =1:2.15	Co:Ni =1:1.06

Table S4. The summary of electrochemical properties of as-fabricated samples and Pt for HER in 1 M KOH.

Sample	η_{10}[a)] [mV]	R_s [Ω]	R_{ct} [Ω]
NiFeCoO	192.4	6.42	37.78
FeCoO	124.4	6.55	25.86
FeNiO	397.4	6.07	344.63
CoNiO	465.4	6.32	442.28
Pt	66	1.19	1.38

η_{10}[a)]: Overpotential (mV *vs* RHE) needed to reach a current density of -10 mA cm^{-2}.

Table S5. The summary of electrochemical properties of NiFeCoO-NF, Ni foam and FeCoO-NF for HER in 1 M KOH.

Sample	η_{10}[a)] [mV]	R_s [Ω]	R_{ct} [Ω]
NiFeCoO-NF	82	7.54	12.1
Ni foam	172.4	6.78	17.4
FeCoO-NF	66	7.18	7.91

η_{10}[a)]: Overpotential (mV *vs* RHE) needed to reach a current density of -10 mA cm^{-2}.

Table S6. The summary of electrochemical properties of NiFeCoO-NF, Ni foam, FeCoO-NF and Pt for HER in 0.25 M Na_2S/0.35 M Na_2SO_3.

Sample	η_{10}[a)] [mV]	R_s [Ω]	R_{ct} [Ω]
NiFeCoO-NF	/	8.04	13.02
Ni foam	/	7.81	39.08
FeCoO-NF	/	7.50	9.18
Pt	/	3.59	3.66

η_{10}[a)]: Overpotential (mV *vs* RHE) needed to reach a current density of -10 mA cm^{-2}.

[1] L. Yang, H. Zhou, X. Qin, X. Guo, G. Cui, A.M. Asiri, X. Sun, Cathodic electrochemical activation of Co_3O_4 nanoarrays: a smart strategy to significantly boost the hydrogen evolution activity, Chem. Commun. (Camb). 54 (2018), 2150-2153, http://dx.doi.org/10.1039/c7cc09416g.

[2] J. Wang, S. Mao, Z. Liu, Z. Wei, H. Wang, Y. Chen, Y. Wang, Dominating role of Ni(0) on the interface of Ni/NiO for enhanced hydrogen evolution reaction, ACS. Appl. Mater. Interfaces. 9 (2017), 7139-7147, http://dx.doi.org/10.1021/acsami.6b15377.

[3] X. Yan, L. Tian, M. He, X. Chen, Three-dimensional crystalline/amorphous Co/Co_3O_4 core/shell nanosheets as efficient electrocatalysts for the hydrogen evolution reaction, Nano. Lett. 15 (2015), 6015-6021, http://dx.doi.org/10.1021/acs.nanolett.5b02205.

[4] Y. Tian, A. Huang, Z. Wang, M. Wang, Q. Wu, Y. Shen, Q. Zhu, Y. Fu, M. Wen, Two-dimensional hetero-nanostructured electrocatalyst of Ni/NiFe-layered double oxide for highly efficient hydrogen evolution reaction in alkaline medium, Chem. Eng. J. 426 (2021), http://dx.doi.org/10.1016/j.cej.2021.131827.

[5] E.C. Lovell, X. Lu, Q. Zhang, J. Scott, R. Amal, From passivation to activation - tunable nickel/nickel oxide for hydrogen evolution electrocatalysis, Chem. Commun. (Camb). 56 (2020), 1709-1712, http://dx.doi.org/10.1039/c9cc07486d.

[6] J. Zhang, X. Shang, H. Ren, J. Chi, H. Fu, B. Dong, C. Liu, Y. Chai, Modulation of inverse spinel Fe_3O_4 by phosphorus doping as an industrially promising electrocatalyst for hydrogen evolution, Adv. Mater. 31 (2019), e1905107, http://dx.doi.org/10.1002/adma.201905107.

[7] H.A. Bandal, A.R. Jadhav, A.H. Tamboli, H. Kim, Bimetallic iron cobalt oxide self-supported on Ni-Foam: An efficient bifunctional electrocatalyst for oxygen and hydrogen evolution reaction, Electrochim. Acta. 249 (2017), 253-262, http://dx.doi.org/10.1016/j.electacta.2017.07.178.

[8] L. Han, L. Guo, C. Dong, C. Zhang, H. Gao, J. Niu, Z. Peng, Z. Zhang, Ternary mesoporous cobalt-iron-nickel oxide efficiently catalyzing oxygen/hydrogen evolution reactions and overall water splitting, Nano. Research. 12 (2019), 2281-2287, http://dx.doi.org/10.1007/s12274-019-2389-5.

[9] H. Jin, J. Wang, D. Su, Z. Wei, Z. Pang, Y. Wang, In situ cobalt-cobalt oxide/N-doped carbon hybrids as superior bifunctional electrocatalysts for hydrogen and oxygen evolution, J. Am. Chem. Soc. 137 (2015), 2688-2694, http://dx.doi.org/10.1021/ja5127165.

[10] B.H.R. Suryanto, Y. Wang, R.K. Hocking, W. Adamson, C. Zhao, Overall electrochemical splitting of water at the heterogeneous interface of nickel and iron oxide, Nat. Commun. 10 (2019), 5599, http://dx.doi.org/10.1038/s41467-019-13415-8.

[11] W. Chu, Z. Shi, Y. Hou, D. Ma, X. Bai, Y. Gao, N. Yang, Trifunctional of phosphorus-doped $NiCo_2O_4$ nanowire materials for asymmetric supercapacitor, oxygen evolution reaction, and hydrogen evolution reaction, ACS. Appl. Mater. Interfaces. 12 (2020), 2763-2772, http://dx.doi.org/10.1021/acsami.9b13182.

[12] C. Xiao, Y. Li, X. Lu, C. Zhao, Bifunctional porous $NiFe/NiCo_2O_4$/Ni Foam electrodes with triple hierarchy and double synergies for efficient whole cell water splitting, Adv. Funct. Mater. 26 (2016), 3515-3523, http://dx.doi.org/10.1002/adfm.201505302.

[13] T. Ling, D.Y. Yan, H. Wang, Y. Jiao, Z. Hu, Y. Zheng, L. Zheng, J. Mao, H. Liu, X.W.

Du, M. Jaroniec, S.Z. Qiao, Activating cobalt(II) oxide nanorods for efficient electrocatalysis by strain engineering, Nat. Commun. 8 (2017), 1509, http://dx.doi.org/10.1038/s41467-017-01872-y.

[14] H.H. El-Maghrabi, A.A. Nada, M.F. Bekheet, S. Roualdes, W. Riedel, I. Iatsunskyi, E. Coy, A. Gurlo, M. Bechelany, Coaxial nanofibers of nickel/gadolinium oxide/nickel oxide as highly effective electrocatalysts for hydrogen evolution reaction, J. Colloid. Interface. Sci. 587 (2021), 457-466, http://dx.doi.org/10.1016/j.jcis.2020.11.103.

[15] M. Gong, W. Zhou, M.C. Tsai, J. Zhou, M. Guan, M.C. Lin, B. Zhang, Y. Hu, D.Y. Wang, J. Yang, S.J. Pennycook, B.J. Hwang, H. Dai, Nanoscale nickel oxide/nickel heterostructures for active hydrogen evolution electrocatalysis, Nat. Commun. 5 (2014), 4695, http://dx.doi.org/10.1038/ncomms5695.

[16] W. Adamson, X. Bo, Y.B. Li, B.H.R. Suryanto, X.J. Chen, C. Zhao, Co-Fe binary metal oxide electrocatalyst with synergistic interface structures for efficient overall water splitting, Catal. Today. 351 (2020), 44-49, http://dx.doi.org/10.1016/j.cattod.2019.01.060.

[17] L.Y. Wang, C.D. Gu, X. Ge, J.L. Zhang, H.Y. Zhu, J.P. Tu, Anchoring Ni_2P sheets on $NiCo_2O_4$ nanocone arrays as optimized bifunctional electrocatalyst for water splitting, Adv. Mater. Interfaces. 4 (2017), http://dx.doi.org/ARTN170048110.1002/admi.201700481.

[18] N. Dalai, B. Mohanty, A. Mitra, B. Jena, Highly active ternary nickel-iron oxide as bifunctional catalyst for electrochemical water splitting, Chemistryselect. 4 (2019), 7791-7796, http://dx.doi.org/10.1002/slct.201901465.

[19] R. Elakkiya, R. Ramkumar, G. Maduraiveeran, Flower-like nickel-cobalt oxide nanomaterials as bi-functional catalyst for electrochemical water splitting, Mater. Res Bull. 116 (2019), 98-105, http://dx.doi.org/10.1016/j.materresbull.2019.04.016.

[20] M.S. Riaz, S.W. Zhao, C.L. Dong, M.J. Iqbal, Y.T. Zhao, F.Q. Huang, Spherical sacrificial ZnO template-derived hybrid Ni/Co_3O_4 cubes as efficient bifunctional electrocatalyst for overall water splitting, Energy. Technol-Ger. 8 (2020), http://dx.doi.org/ARTN 190131010.1002/ente.201901310.

[21] Y.M. Xie, X.F. Wang, K. Tang, Q. Li, C.L. Yan, Blending Fe_3O_4 into a Ni/NiO composite for efficient and stable bifunctional electrocatalyst, Electrochim. Acta. 264 (2018), 225-232, http://dx.doi.org/10.1016/j.electacta.2018.01.136.

[22] L.M. Tao, Y.B. Li, M. Li, G.Y. Gao, X. Xiao, M.K. Wang, X.X. Jiang, X.W. Lv, Q.W. Li, S.S. Zhang, Z.X. Zhao, C. Zhao, Y. Shen, Nanostructured nickel cobaltite antispinel as bifunctional electrocatalyst for overall water splitting, J. Phys. Chem. C. 121 (2017), 25888-25897, http://dx.doi.org/10.1021/acs.jpcc.7b08814.

[23] J. Cao, X.B. Chen, H.C. Li, J.X. Pu, L.M. Liu, L. Ma, K.C. Zhou, Z.J. Zhang, Q.P. Wei, F.H. Luo, A Co/CoO hybrid rooted on carbon cloth as an efficient electrocatalyst for the hydrogen evolution reaction in alkaline solution, Sustain. Energ. Fuels. 4 (2020), 1924-1932, http://dx.doi.org/10.1039/c9se01128e.